ACS APPLIED NANO MATERIALS

www.acsanm.org Article

Dual-Mode Colorimetric Sensor Based on Ultrathin Resonating Facilitator Capable of Nanometer-Thick Virus Detection for Environment Monitoring

Young Jin Yoo,$^\nabla$ Joo Hwan Ko,$^\nabla$ Won-Guen Kim,$^\nabla$ Yeong Jae Kim, Duk-Jo Kong, Seungchul Kim, Jin-Woo Oh,* and Young Min Song*

Cite This: https://dx.doi.org/10.1021/acsanm.0c01067 Read Online

ACCESS | Metrics & More | Article Recommendations | Supporting Information

ABSTRACT: Endowed structural colors in some living organisms provide inspiration for alterable colors depending on the surrounding environment. Although many structural designs for surrounding sensitive colors for various analytes have been introduced, practical applications in a variety of environments require a unified design that can cover the key optical influences of external environmental changes. A bimodal approach to colorimetric sensor design for optimization on different environmental stimuli is presented, based on a single platform composed of a highly lossy medium and a metal. A dual-mode colorimetric facilitator (DMCF) is optimally designed on the basis of the spectral response for each mode depending on the refractive index and thickness, which are optical key elements of changes in the surrounding environment. DMCFs with aqueous solutions and oxide layers are experimentally verified for different refractive indices and thicknesses in nanometer scale. As a biomaterial application, minute in nanometer-thick changes of the virus coated on DMCF are distinguished by color differences. For intuitive recognition of environmental change, the colorimetric indicator is designed as a separate insensitive/sensitive area to reveal hidden patterns beyond a certain thickness of the coated virus in nanometer thick. For scalability/flexibility, a large-area flexible sample is also fabricated on a wafer scale.

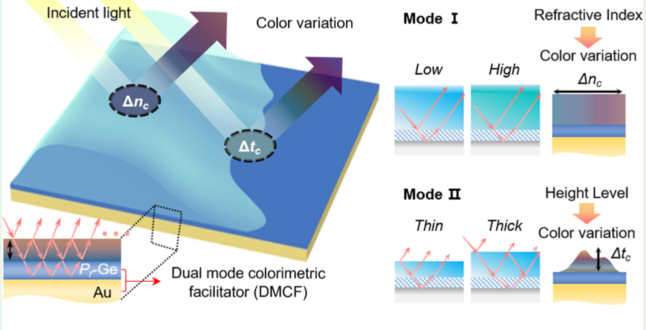

KEYWORDS: *colorimetric sensor, external environment detection, refractive index sensing, virus detection, thin-film coloration*

Innate structural features, which are observed in certain nature creatures such as butterflies and beetles, cause brilliant colors depending on the surrounding environment.[1,2] These concomitant colors arise from visible light interference caused by micro-/nanoscale structures that are optically affected by the external circumstance.[3−5] Recently, various pollutants released as a result of ongoing industrialization and urbanization require a complex surrounding monitoring to aid medical diagnosis, environmental surveillance, homeland protection, and other applications.[6,7] Hence, surrounding dependency of structural coloring schemes, which were inspired by nature, provides possibilities for visualization of diverse environmental changes.[8,9]

With recent advances in photonic structures, particular structural colors can be sensitively altered depending on the external stimuli.[10,11] On the basis of natural photonic structures, specific examples of photonic crystal based colorimetric sensors show unprecedented potential for practical sensing of temperature, pH, ion species, solvents, water vapor, humidity, pressure, and biomolecules.[12−18] A combination of introduced design methods for colorimetric detection, inspired by photonic structures, relies on highly ordered and/or periodically arranged structures; thus, enormous structural and/or material modifications are involved to cover various environmental changes affecting optical key factors such as refractive index (RI) and thickness.[19−21] Moreover, co-assembling of multiple materials and micro-/nano building blocks to achieve uniform colors at a large scale constrains their rapid/convenient fabrication. As a simple structural approach, surrounding-dependent color alterations based on the principle of thin-film interference, such as Bragg reflectors and plasmonic resonators, have been demonstrated for a wide range of external environments. Nonetheless, colorimetric detection strategies based on photonic take a wide variety of forms including thin-films, and porous structures for different analytes.[22−25] Realistic

Received: April 21, 2020
Accepted: June 5, 2020
Published: June 5, 2020

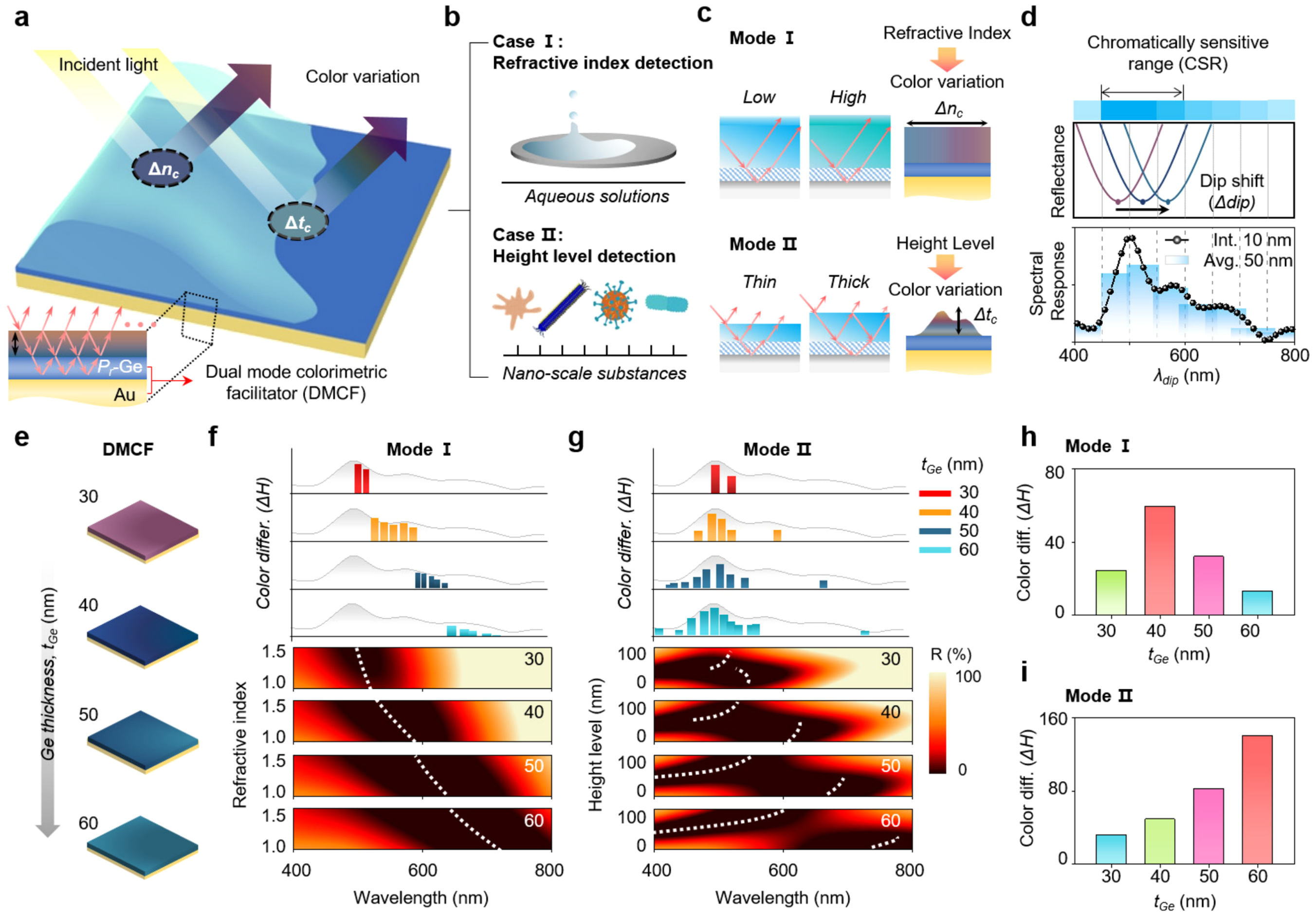

Figure 1. (a) Schematic illustration of dual-mode colorimetric facilitator (DMCF) with color variation corresponding to refractive index (RI) and thickness change of coating layer. (b) Concept schemes for detecting cases of aqueous solution detection (case I) and nanoscale substance detection (case II), respectively. (c) Schematic of colorimetric sensing mechanism with DMCF for refractive index changes (Δn_c) (mode I) and nanometer-scale fine thickness variations (Δt_c) (mode II). (d) Chromatically sensitive range (CSR) corresponding to dip position shift through 400−800 nm. (e) Schematic image and origin color of DMCF for different P_r-Ge thickness (t_{Ge}) (30−60 nm). (f) Calculated color differences (ΔH) corresponding to dip shift with spectral response as a background and reflectance contours of DMCFs to Δn_c (1.0−1.5) for mode I. Each column interval represents 15 nm Δdip range. White dashed lines represent dip position. (g) Calculated color difference and contours obtained in the same way for mode II Δt_c (0−100 nm). (h, i) Total color differences (ΔH) for (h) mode I and (i) mode II integrated from each column in color differences (ΔH) of panels f and g, respectively.

applications in a variety of environments require the provision of consistent design rules, and elements with optimization of structure and chromaticity that are applicable in multiple analytes on a single platform, as in other nonphotonic structure based colorimetric detections.[25−29]

Herein, we present a unified platform for colorimetric sensor design to convertibly optimize for different environmental stimuli. As a simple and effective structure, an ultrathin-film structure was exploited to design a dual-mode colorimetric facilitator (DMCF). By combining a metal with a highly absorbent dielectric, strong optical interference within considerably thinner thickness can be obtained compared to that of a conventional coating layer due to nontrivial phase change of reflected waves. By these properties, a resonance behavior affecting the structural color was observed in a structure composed of an ultrathin absorbing layer (Ge) on a metal substrate (Au).[30−32] On the basis of the extraordinary optical sensitivity with nontrivial interface phase changes with the external medium, the proposed structure is optimized without significant structural modifications based on the spectral response for each mode according to the RI and thickness, which are the main optical factors that respond to the surrounding environmental changes. Optimized structures for each mode are experimentally verified for different RIs and thicknesses through aqueous solution dropping and additional oxide layer deposition. As a specific application in biomaterials, we demonstrate virus detection by distinguishing the small thickness variation of the coated virus by color differences of the proposed structure in nanometer scale. For practical demonstration with selective chromatic sensitivity, the colorimetric indicator designed as separate insensitive/sensitive areas reveals hidden patterns above the specific thickness of the coated virus, allowing intuitive perception of environmental changes. For scalability/flexibility, we also fabricate a large-area flexible sample at a wafer scale. Furthermore, colorimetric properties of the proposed structure will be discussed with conventional substrates.

■ RESULTS AND DISCUSSION

Basic Concept of Dual-Mode Colorimetric Facilitator. Figure 1a shows a schematic of dual-mode colorimetric sensing with changes in RI or thickness. To implement structurally

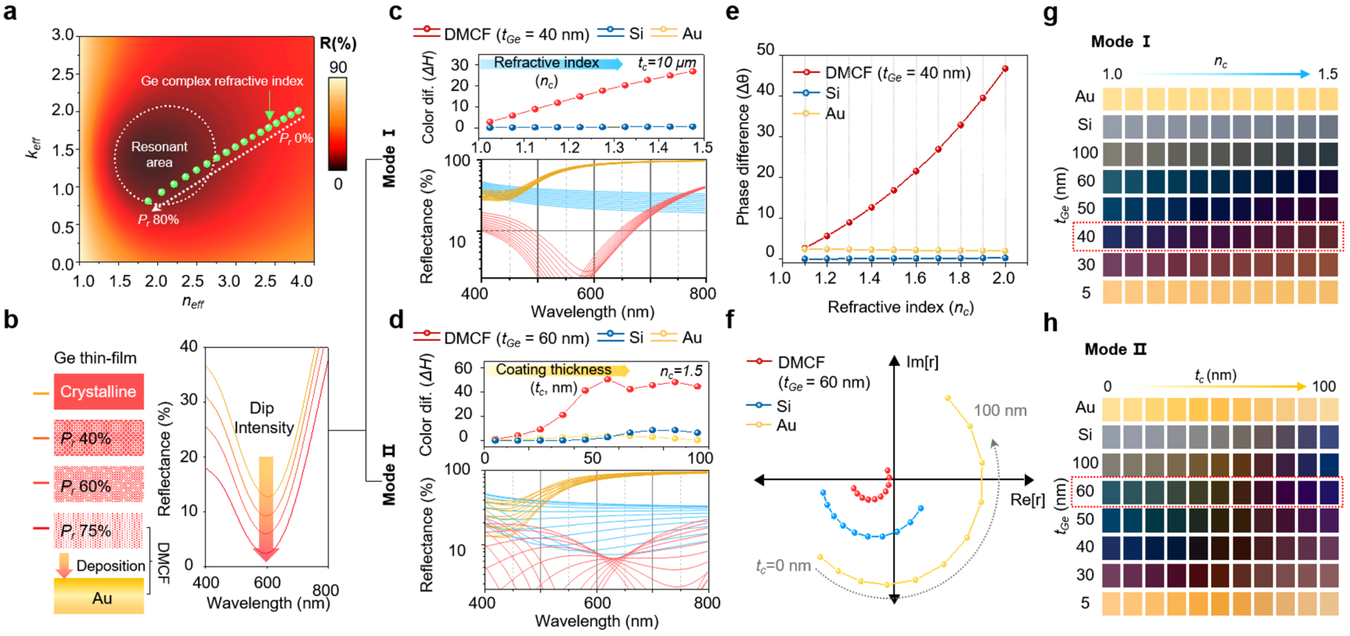

Figure 2. (a) Reflectance contour of resonant layer/Au structure corresponding to complex refractive index combinations at λ = 600 nm. The center circle represents the resonant area. (b) Simulated reflectance spectra of Ge/Au structures with various porosities having the same dip position (λ = 600 nm), P_r 0%/13 nm, 40%/20 nm, 60%/29 nm, and 75%/41 nm. (c, d) Color difference and calculated reflectance spectra of (c) Δn_c (1.0−1.5) and (d) Δt_c (0−100 nm) for the DMCF, Si, and Au substrates. (e) Phase differences diagram for Δn_c (1.0−2.0) of coating layer on the DMCF (t_{Ge} = 40 nm), Si, and Au. (f) Reflection coefficient trajectory of DMCF (t_{Ge} = 60 nm), Si, and Au, respectively, for Δt_c (0−100 nm) of coating layer. (g, h) Calculated color palettes in accordance with (g) Δn_c (1.0−2.0) and (h) Δt_c (0−100 nm) as an external refractive index for DMCF, Si, and Au substrates.

simple colorimetric detection, we designed a DMCF composed of a highly lossy medium (P_r-Ge) and a metal substrate (Au). For dual-mode colorimetric detection, external environmental changes of two different cases were considered with aqueous solutions (case I) and nanoscale substances (case II) on DMCF (Figure 1b). In case I and case II, the main factors affecting colorimetric detection are RI and thickness, respectively. For dual-mode optimization, in mode I, a bulky external layer with refractive index changes (Δn_c) on DMCF was considered, and in mode II, an external layer with nanometer-scale fine thickness variations (Δt_c) on DMCF was considered (Figure 1c).

For consistency of optimization in both modes, we adopted a spectral response derived from color matching functions. Figure 1d shows the spectral response calculated by dip shift in the visible wavelengths based on the reflective color scheme (see Figure S1, Supporting Information, for details). The result shows a relatively high spectral response in a specific wavelength range (λ_{dip} = 450−600 nm), which means that achieving a dip shift in this chromatically sensitive range (CSR) allows for drastic color changes.[33] For comparison in each mode, we calculated reflectance and corresponding color difference (ΔH) with changes in RI and fine thickness on DMCFs of different thicknesses (t_{Ge} = 30−60 nm), as shown in Figure 1e. As a result of mode I with Δn_c, the dip shift range of DMCF with t_{Ge} = 40 nm is most coincident with CSR, resulting in relatively high values of color difference (ΔH) (Figure 1f). In the result of mode II with Δt_c, although dip shifts of all DMCFs coincide with CSR, especially, DMCF of t_{Ge} = 60 nm showed the widest dip shift range (Figure 1g). In both modes, the distributions of color differences are similar to the tendency of the spectral response from the color matching function. For quantitative evaluation, we conducted integration of the color difference values on DMCFs of different thickness (t_{Ge} = 30−60 nm) in each mode (Figure 1h,i). From the results, we noted that outstanding colorimetric properties on a single platform for refractive index and thickness variations, with the highest integrated values at t_{Ge} = 40 nm in mode I and t_{Ge} = 60 nm in mode II.

Colorimetric Principle of DMCF. As a cornerstone to achieve colorimetric detection, Figure 2a shows a computational optimizing process to define a resonant condition with reflectance contour map versus complex refractive index at a specific wavelength (λ = 600 nm). As indicated, the reflectance shows a minimum value at a specific resonant area which is a crucial point enhancing light absorption for more sensitive chromatic change. (Figure S2, Supporting Information). In this study, the optical constants were modulated by applying porosity (P_r) to the Ge thin film for approaching toward resonant area, in order to enhance chromaticity with light absorption of the reflective resonant structure following the subtractive color mechanism (see Figure S3, Supporting Information, for color purity comparison).[31,34,35] As a result, the dip intensity of the reflectance spectrum decreased from 13% to 2% by applying P_r 75% to the Ge thin film, consequently, an ultrathin layered structure of P_r 75% Ge layer with Au reflector was selected for use as the DMCF (Figure 2b).

For a confirmation of enhanced chromatic responses of the DMCF compared with conventional substrate, color differences were considered within ranges of Δn_c (1−1.5) and Δt_c (0−100 nm) for DMCF, Au, and Si substrate (Figure 2c,d; see Figure S4, Supporting Information, for details). As depicted, in the case of DMCF, the dip intensity of each spectrum was formed close to zero reflectance (see Figure S5, Supporting Information, for details). Following this tendency, only DMCF

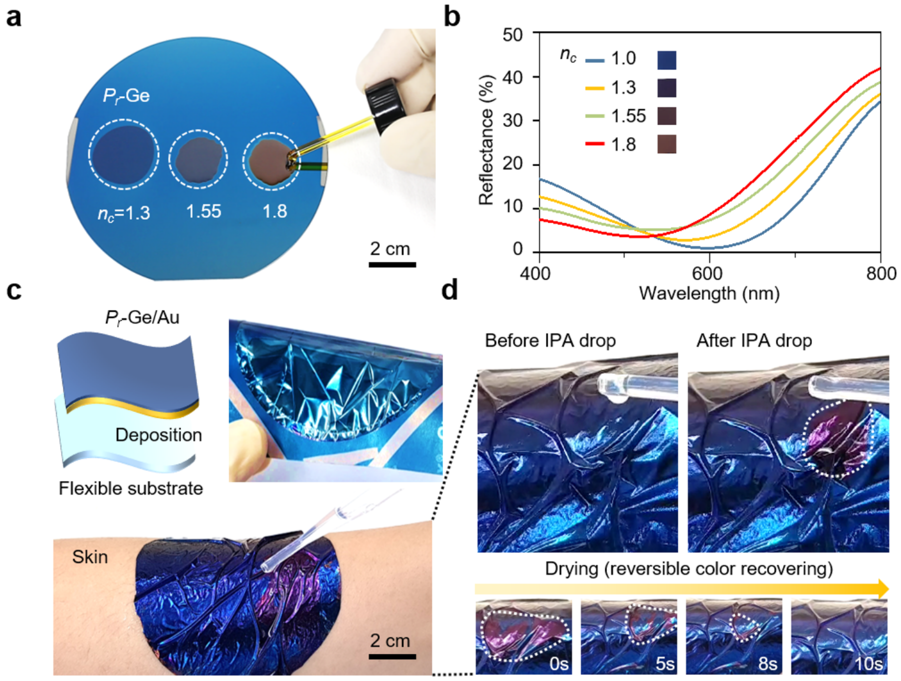

Figure 3. (a) Photographic image of various color responses with solution drop for different Δn_c (1.3, 1.55, and 1.8) of DMCF. (b) Measured reflectance spectra of solution-coated DMCF for different Δn_c (1.0, 1.3, 1.55, and 1.8). (c) Schematic illustration (upper left) and fabricated sample image (upper right) of flexible DMCF attached on human skin (bottom). (d) External environment detecting process with IPA (n_c = 1.38) solution drop and sequential images of the reversible color recovery process.

showed distinct color differences (ΔH), whereas another substrate showed no significant difference from its own original color (see Figure S6, Supporting Information, for details). Furthermore, to analyze the effect of each substrate with regard to forming a drastic color change, the surface reflection processes were considered for both dual modes (see Figure S7, Supporting Information, for details). As shown in Figure 2e, since complex refractive index of P_r-Ge was modulated to lowering, the phase of reflection coefficient (r_0) changed sensitively, which dominantly affects the total amount of reflection (see Figure S8, Supporting Information, for details). Consequently, this sensitive phase change enables noticeable sensing ability compared with the other substrates. In the case of mode II for additional layer thickness changes (t_c = 0−100 nm), due to the similar RI between additional layer (n_c = 1.5) and P_r-Ge (n_{Ge} ∼ 2), the r_1 of DMCF approaches the origin point closer than other substrates, causing a sensitive color change with large resonance (Figure 2f; see Figure S9, Supporting Information, for details).[36] As a comprehensive and intuitive comparison in colorimetric sensing capabilities, RGB color palettes were presented that exhibit sensitive/insensitive color change corresponding to substrates with varying t_{Ge} (Figure 2g,h; see Table S1 and Figures S10 and S11,Supporting Information, for details). Consequently, as designed by chromatic comparison before, the most distinct color change was observed at t_{Ge} = 40 nm for mode I and t_{Ge} = 60 nm for mode II. Depending on the material combination of the DMCF, we also confirmed the chromaticity values are widely or locally varied with t_{Ge} and n_c change (see Figures S12 and S13, Supporting Information, for details).

Aqueous Solution Detection. For an experimental confirmation of RI detecting to outward substances with different Δn_c of aqueous solution (1−1.8), Figure 3a shows a RGB image of aqueous solution coated DMCF (t_{Ge} = 40 nm) with different color responses corresponding to each refractive index liquids (series AAA (n = 1.3), series A (n = 1.55), series A (n = 1.8), Cargille, USA). On the basis of these visibly distinguishable results, for more quantitative estimation, reflectance was measured (Figure 3b). Since this color variation was originated by the reflection phase change in accordance with Δn_c of an external aqueous layer, the RI of the aqueous solution can be estimated by chromatic matching (see Figure S14, Supporting Information, for details). As the RI of the aqueous solution increases, the dip position shifted from 600 nm to a shorter wavelength range (see Figure S15, Supporting Information, for details). To enhance the applicability in daily life, DMCF was prepared on a polyester thin film (t = 2.5 μm) as a flexible substrate (Figure 3c, top). Due to ultrathin dimensions and angle robustness, DMCF enables applying the flexible colorimetric sensor to any arbitrary surface with improved sensing reliability (Figure 3c, bottom). Figure 3d shows a fabricated sample of a flexible colorimetric sensor with aqueous solution detector. Without any drop of solution on the surface, the DMCF shows a conformal color uniformity over whole area. However, after application of an isopropyl alcohol (IPA) drop, the area covered with solution changes color, enabling prediction of the coated solution information. Furthermore, the color variation occurred due to the resonance conditions change affected by external environment, the color response appeared immediately. After the IPA evaporated, the color of DMCF reversibly returned to its original color (see Movie S1, Supporting Information, for an immediate color change and reversible color recovery process). Additionally, to figure out the sensing capability for both high and low surface energy solvents, we measured contact angle and confirmed intuitive and observable colors for various solutions, whether high or low surface energy (see Figure S16, Supporting Information, for details).

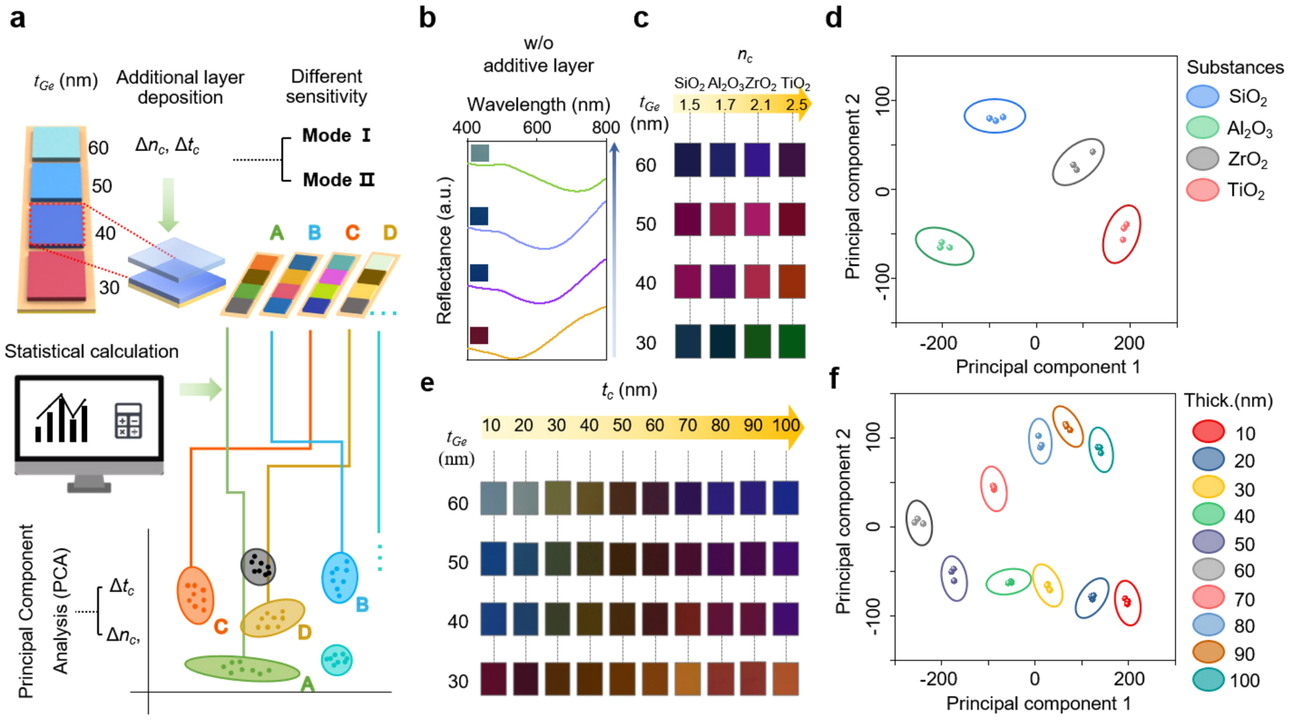

Figure 4. (a) Schematic illustration of colorimetric sensor array with different t_{Ge} (30−60 nm) and the analyzing process for statistical detection of mode I and mode II for a deposited additional layer (top). Clustering process from the colorimetric sensor array to separated group by principal component analysis (PCA) method. (b) Measured reflectance spectra and captured RGB image of each colorimetric sensor corresponding to t_{Ge} (30−60 nm). (c) Color patterns of fabricated colorimetric sensor array with converted RGB difference from the origin color (under $n_c = 1$) to additional layers (n_c = 1.5, 1.7, 2.1, and 2.5) of SiO_2, Al_2O_3, ZrO_2, and TiO_2, respectively. The additional layer is deposited with t_c of 50 nm for each substance. (d) PCA result of additional layer of panel c as mode I. (e) Color patterns of fabricated colorimetric sensor array with RGB value for additional layers (t_c = 10−100 nm of SiO_2). (f) PCA result of additional layer of panel e as mode II.

Statistical Sensing with Principal Component Analysis. To realize more accurate sensing result for diverse substances, we used a principal component analysis (PCA) and introduced a colorimetric sensor array with different sensitivity for each pixel. As each DMCF in colorimetric sensor array has different color responses to Δn_c and Δt_c, the colorimetric sensor array showed diverse color combinations at each modes. Figure 4a shows a schematic illustration of the detecting/analyzing process of the colorimetric sensor array by deposition of an additional layer having different RI or thickness for mode I and mode II, respectively. For a quantitative classification, PCA was performed as a statistical clustering method using acquired total RGB combinations from each pixel. The created subspaces consist of the same group corresponding to Δn_c and Δt_c for mode I and mode II, respectively. For experimental confirmation, we fabricated a colorimetric sensor array with four DMCFs (t_{Ge} = 30−60 nm) and their reflectance spectra show each pixel has different initial dip position and color (Figure 4b). On the basis of the DMCF array, an additional layer was deposited on different substances (SiO_2, Al_2O_3, ZrO_2, and TiO_2) with different Δn_c (1.5, 1.7, 2.1, and 2.5), respectively (see Figure S17, Supporting Information for detail). From these samples, the difference in color was converted by the RGB disparity from the basis of initial substrate color (Figure 4c; see Figure S18, Supporting Information, for details). Figure 4d shows a two-dimensional (2D) PCA result from the achieved RGB information and the first two principal components show a large variance in the four substances, which was successfully clustered into subspaces, as a Δn_c detector for mode I. For an experimental confirmation of mode II, the DMCF array was deposited with SiO_2 (n_c = 1.5) to different Δt_c (0−100 nm), showing a diverse color combination (Figure 4d). From this RGB information, the PCA was calculated (Figure 4f), and the first two principal components show a large variance over the ten discrete Δt_c and were successfully separated into subgroups.

Surface Height Level Profiling. As another practical application, surface thickness profiling in nanoscale substances was performed for several differently shaped additional layers. For a quantitative comparison, the calculated/measured reflectance spectra were compared by considering the dip position and intensity (Figure S19, Supporting Information). On the basis of this result, to estimate the thickness of the round-shaped structure, Figure 5a represents overdeveloped photoresist (PR) patterns. This microdot pattern shows color distribution at the side edge. Since this color variation was originated by the reflection coefficient trajectory closing toward the origin corresponding to Δt_c of the external substance layer, the thickness of the additional layer can be estimated by chromatic matching (Figure 5b; see Figure S20, Supporting Information, for details). For experimental confirmation, the estimated Δt_c, the pattern surface was measured by atomic force microscopy (AFM). Converted from the graded level, both the estimated and measured coating layer thickness were well matched to each other over the vertical range from a few nanometers to a hundred nanometers (Figure 5c; Figures S21 and S22, Supporting Information). For an experimental confirmation in the case of an arbitrary surface, the partially dropped virus (M13 phage) was spin-

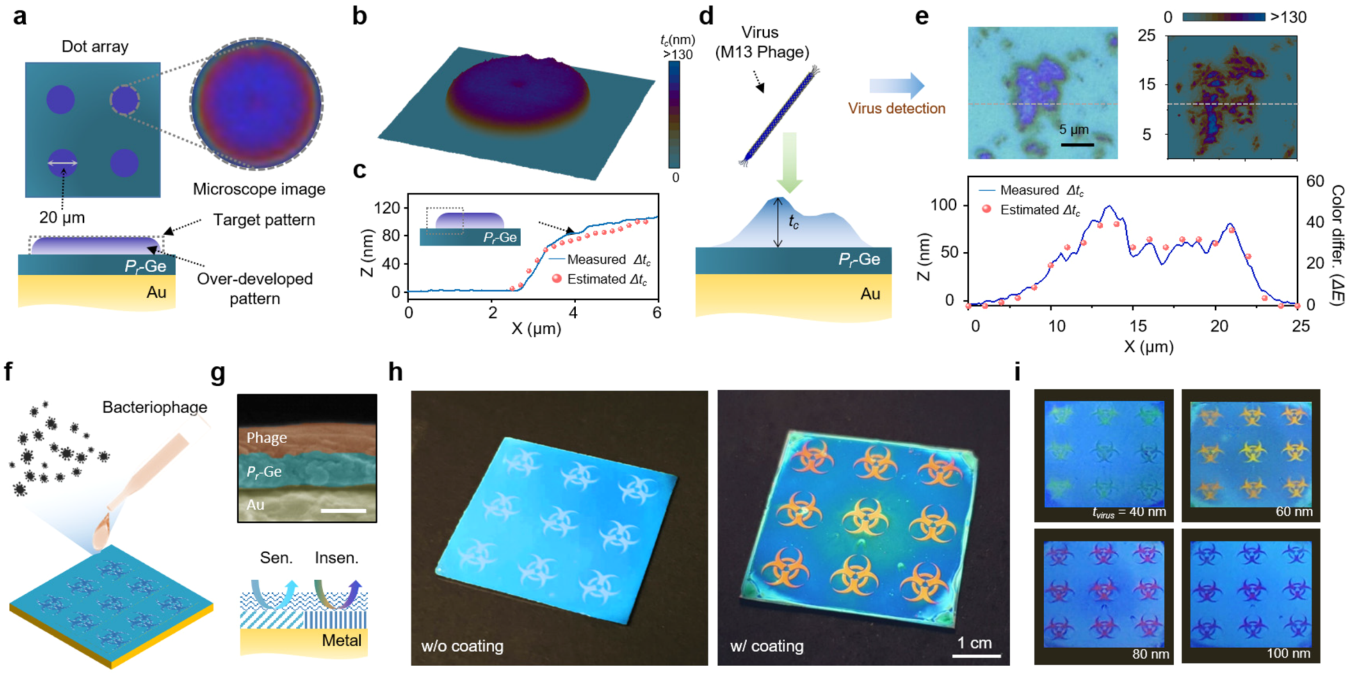

Figure 5. (a) Schematic image of overdeveloped micro-photoresist dots and bright-field image with color variation at side edges. (b) 3D AFM image with graded color map of the DMCF with t_{Ge} = 60 nm. (c) Thickness of overdeveloped pattern measured by AFM and estimated Δt_c. (d) Schematic illustration of M13 phage virus coating process and their arbitrary surface. (e) Colorimetric virus detection result of the M13 phage. Bright-field image (upper left) and 3D AMF image marked with color map (upper right) and measured/estimated H.L. over the marked dashed line (bottom). (f) Schematic of patterned virus indicator with visualization process by coating the phage layer onto insensitive/sensitive areas (left). (g) SEM image of phage-coated DMCF (top) and the areal design of virus indicator (bottom). (h) Color images of patterned virus indicator in different states (before coating/after coating). Virus thickness (t_{virus}) is 60 nm. (i) Color images of phage-coated virus indicator with t_{virus} (40−100 nm).

coated onto DMCF (Figure 5d).[37] As stacking M13 phage film, the thickness of the thin film increasing (see Figure S23, Supporting Information, for details). Almost every optical sensor fabricated with M13 phage-based thin films is formed in thickness of tens to hundreds of nanometers during self-assembly process.[37] For this reason, DMCF can be an excellent method to provide facile and intuitive estimation of the thickness of M13 phage-based thin film. The virus-coating layer shows an irregular nanoscale thickness indicated by color variation (Figure 5e, top). On the basis of the calculated color difference from virus-coating layer, the displayed color was graded into thickness level, which closely matched the AFM results (Figure 5e; see Figure S24, Supporting Information, for material information on the M13 phage).

For an intuitive observation with the naked eye, we designed a large-area virus indicator using selective chromatic responsivity. Figure 5f shows a schematic of the virus indicator with patterns which are dependent on the virus thickness (t_{virus}) (see Figure S25, Supporting Information, for details). The virus solution dropped on the entire surface was spin-coated with uniform thickness (Figure 5g, top). The patterned area was designed to have insensitive or sensitive response to an additional layer. Due to the high RI of Ge of P_r 0%, the background area is insensitive to an additional layer, resulting in only the patterned area reacting, corresponding to t_{virus} (Figure 5f, bottom; see Figure S26, Supporting Information, for details). Figure 5h shows sample images of a virus indicator fabricated by a conventional photolithographic process. Without a virus coating, the symbol showed a similar color with background (Figure 5h, left). However, virus-coated DMCF revealed a distinct color pattern (Figure 5h, right). Furthermore, in accordance with t_{virus}, the pattern color showed different colors enabling detecting of the virus thickness over a large area (Figure 5i; see Figure S27, Supporting Information, for details). Finally, from these results, we confirmed the DMCF is stable for a conventional lithography process under high temperature (120 °C) and, after processing, the sensing ability is conserved and even reusability was confirmed after washing with DI water (Figures S28 and S29, Supporting Information,for details).

■ CONCLUSIONS

We presented a consistent strategy for colorimetric sensor design capable of optimization with a single parameter according to different external stimuli. The dual-mode colorimetric facilitator (DMCF), which was optimized by chromatically spectral response, showed sensitive chromatic responsiveness for both refractive index and thickness change. The fabricated DMCFs were confirmed to have selective colorimetric properties in each mode according to refractive index and thickness changes by dropping aqueous solutions and depositing oxide layers. As a biomaterial application, we successfully demonstrated nanoscale virus detection with thickness estimation by comparing color difference values. Moreover, for practicality, we demonstrated a colorimetric sensor, indicating external environment changes by revealing a specific spatially designed pattern with selective chromatic responsivity in nanometer scale. The proposed bimodal detection on a single photonic platform for different environmental changes will open up expanded possibilities in colorimetric environmental detection and surrounding dependent colors. In addition, we expect that our design scheme with chromatically spectral responsiveness will be an effective and powerful means to achieve sensitive color alteration. Furthermore, we believe that the proposed structure will provide a universal platform for a variety of target-specific applications with additional surface treatment for selective detection.[38,39]

EXPERIMENTAL SECTION

Optical Calculation. RCWA was used to calculate reflectance of DMCF and conventional substrate for mode I and mode II using commercial software (DiffractMOD, RSoft Design Group, USA).[40] In the RCWA, the simulation conditions were set to the second diffraction order for diffraction efficiency and grid size was set to 0.2 nm, which was sufficient to numerically stabilize the results. In addition, material dispersion and extinction coefficients were considered to obtain accurate output. The commercial software MATLAB (MathWorks, USA) was used to calculate the effective complex refractive index based on the volume average theory (VAT) and chromatic output from calculated/measured reflectance.[34]

Optical Characterization. The reflectance spectra of the fabricated samples were measured by a UV−vis−near-IR spectrometer (Cary 500, Varian, USA) using a tungsten−halogen lamp light source with a normal incident angle. The optical constants were obtained by an ellipsometer (RC2, J.A. Woollam Co., USA) using a He−Ne laser as the source. To obtain RGB intensities for the PCA, each pixel of colorimetric sensor array was captured by CCD camera and converted into RGB intensities. In this study, each pixel captured three times, repeatedly.

Preparation of DMCF. The DMCF ultrathin film was prepared by glancing angle deposition (GLAD) to obtain a porous medium.[41,42] As the substrate, a single polished silicon (100) wafer was selected and treated with a buffer oxide etchant to remove the native oxide layer. Subsequently, each sample was sonicated for 5 min each in acetone, then methanol, and finally deionized water. For flexible samples, a commercial 2.5 μm thick polyester thin film (SpectroMembrane, Chemplex Industries, Inc., Palm City, FL, USA) was used. For stable deposition, the flexible film was attached to a Si substrate. The metal reflector (Au) and absorber layer (Ge) of DMCF were deposited by electron beam evaporation (KVE-E2000, Korea Vacuum Tech Co., Korea.) under high vacuum ($\sim 10^{-6}$ Torr). The Au film was deposited to thickness of 100 nm at a rate of ∼ 2 Å/s, which is sufficient as a metal reflector. The Au-coated layer was mounted on an inclined sample holder (customized) and porous Ge layer deposited to a target thickness with a rate of ∼2 Å/s. For thickness uniformity over the large-scale substrate, GLAD was performed until half of the target thickness, then e-beam flux was temporarily paused, the sample was reloaded upside down 180°, and deposition was resumed. As a result, the DMCF shows a flat surface with conformal color over 4 in. wafer scale (see Figure 3a for an experimental confirmation).[43] The optical constants of DMCF were estimated from the fabricated sample by matching the complex refractive index and porosity (see Figure S30, Supporting Information, for details).

Fabrication of Virus Indicator. To fabricate patterned DMCF, conventional photolithography was used with image reversal photoresist (AZ 5214, AZ Electronic Materials, Luxembourg). The image reversal process was performed with a mask aligner (MJB3 UV400, Karl Suss, Germany) and virus symbol patterned photomask. In each area, a Ge layer was deposited for a porous medium and normal deposition was performed to obtain a dense medium, which show a sensitive or insensitive response, respectively, to additional layer deposition.

Preparation of M13 Phage Solution. To prepare the M13 phage solution, a typical mass amplification protocol was utilized. After mass amplification, M13 phage solution was purified and concentrated via a centrifuge-based washing process. A concentration of the purified M13 phage solution was determined by Beer−Lambert law. Absorbance of M13 phage solution was measured by UV−vis spectrometer (EVO300PC, Thermo Fisher Scientific, Waltham, MA, USA). Prior to spin-coating, dilution or poly(ethylene glycol) (PEG) precipitation method was utilized to achieve the desired concentration of M13 phage solution.

ASSOCIATED CONTENT

Supporting Information

The Supporting Information is available free of charge at https://pubs.acs.org/doi/10.1021/acsanm.0c01067.

Notes of chromatic calculation method and reflection process and schematic illustrations for detail result of fabricated/calculated structure (Figures S1−S30) (PDF)

Movie S1 showing color change by aqueous solution (MP4)

AUTHOR INFORMATION

Corresponding Authors

Young Min Song − *School of Electrical Engineering and Computer Science, Gwangju Institute of Science and Technology, Gwangju 61005, Republic of Korea;* orcid.org/0000-0002-4473-6883; Email: ymsong@gist.ac.kr

Jin-Woo Oh − *Department of Nano Fusion Technology, Department of Nanoenergy Engineering, and BK21 PLUS Nanoconvergence Technology Division, Pusan National University, Busan 46241, Republic of Korea;* orcid.org/0000-0002-0065-5088; Email: ojw@pusan.ac.kr

Authors

Young Jin Yoo − *School of Electrical Engineering and Computer Science, Gwangju Institute of Science and Technology, Gwangju 61005, Republic of Korea;* orcid.org/0000-0002-6490-2324

Joo Hwan Ko − *School of Electrical Engineering and Computer Science, Gwangju Institute of Science and Technology, Gwangju 61005, Republic of Korea;* orcid.org/0000-0001-8129-4319

Won-Guen Kim − *Department of Nano Fusion Technology, Pusan National University, Busan 46241, Republic of Korea;* orcid.org/0000-0003-1485-0551

Yeong Jae Kim − *School of Electrical Engineering and Computer Science, Gwangju Institute of Science and Technology, Gwangju 61005, Republic of Korea;* orcid.org/0000-0002-0870-9044

Duk-Jo Kong − *Advanced Photonics Research Institute, Gwangju Institute of Science and Technology, Gwangju 61005, Republic of Korea;* orcid.org/0000-0001-8674-8981

Seungchul Kim − *Department of Optics and Mechatronics Engineering, Pusan National University, Busan 46241, Republic of Korea;* orcid.org/0000-0002-6765-2471

Complete contact information is available at: https://pubs.acs.org/10.1021/acsanm.0c01067

Author Contributions

$^{\nabla}$Y.J.Y., J.H.K., and W.-G.K. contributed equally to this work.

Notes

The authors declare no competing financial interest.

ACKNOWLEDGMENTS

This work was supported by the National Research Foundation of Korea (NRF) funded by the Korean government (MSIP) (Grants NRF-2017M3D1A1039288, NRF-2018R1A4A1025623, NRF-2018M3D1A1058997, and NRF-2020R1A2C2004983) and the GIST Research Institute (GRI) grant funded by the GIST in 2020. Y.J.Y.. acknowledges the support from the NRF (Grant NRF-2018H1A2A1060954).

■ REFERENCES

(1) Potyrailo, R. A.; Ghiradella, H.; Vertiatchikh, A.; Dovidenko, K.; Cournoyer, J. R.; Olson, E. Morpho butterfly wing scales demonstrate highly selective vapour response. *Nat. Photonics* **2007**, *1*, 123−128.

(2) Vigneron, J. P.; Pasteels, J. M.; Windsor, D. M.; Vértesy, Z.; Rassart, M.; Seldrum, T.; Dumont, J.; Deparis, O.; Lousse, V.; Biró, L. P.; Ertz, D.; Welch, V. Switchable reflector in the Panamanian tortoise beetle Charidotella egregia (Chrysomelidae: Cassidinae). *Phys. Rev. E* **2007**, *76*, No. 031907.

(3) Crookes, W. J.; Ding, L.-L.; Huang, Q. L.; Kimbell, J. R.; Horwitz, J.; McFall-Ngai, M. J. Reflectins: The Unusual Proteins of Squid Reflective Tissues. *Science* **2004**, *303*, 235−238.

(4) Kou, D.; Ma, W.; Zhang, S.; Lutkenhaus, J. L.; Tang, B. High-Performance and Multifunctional Colorimetric Humidity Sensors Based on Mesoporous Photonic Crystals and Nanogels. *ACS Appl. Mater. Interfaces* **2018**, *10*, 41645−41654.

(5) Diao, Y. Y.; Liu, X. Y.; Toh, G. W.; Shi, L.; Zi, J. Multiple Structural Coloring of Silk-Fibroin Photonic Crystals and Humidity-Responsive Color Sensing. *Adv. Funct. Mater.* **2013**, *23*, 5373−5380.

(6) Tang, S.; Li, Y.; Huang, H.; Li, P.; Guo, Z.; Luo, Q.; Wang, Z.; Chu, P. K.; Li, J.; Yu, X.-F. Efficient Enrichment and Self-Assembly of Hybrid Nanoparticles into Removable and Magnetic SERS Substrates for Sensitive Detection of Environmental Pollutants. *ACS Appl. Mater. Interfaces* **2017**, *9*, 7472−7480.

(7) Zhang, Y.-n.; Niu, Q.; Gu, X.; Yang, N.; Zhao, G. Recent progress on carbon nanomaterials for the electrochemical detection and removal of environmental pollutants. *Nanoscale* **2019**, *11*, 11992−12014.

(8) Diao, Y. Y.; Liu, X. Y.; Toh, G. W.; Shi, L.; Zi, J. Multiple Structural Coloring of Silk-Fibroin Photonic Crystals and Humidity-Responsive Color Sensing. *Adv. Funct. Mater.* **2013**, *23*, 5373−5380.

(9) Hong, W.; Chen, Y.; Feng, X.; Yan, Y.; Hu, X.; Zhao, B.; Zhang, F.; Zhang, D.; Xu, Z.; Lai, Y. Full-color CO_2 gas sensing by an inverse opal photonic hydrogel. *Chem. Commun.* **2013**, *49*, 8229−8231.

(10) Qin, M.; Sun, M.; Bai, R.; Mao, Y.; Qian, X.; Sikka, D.; Zhao, Y.; Qi, H. J.; Suo, Z.; He, X. Bioinspired Hydrogel Interferometer for Adaptive Coloration and Chemical Sensing. *Adv. Mater.* **2018**, *30*, 1800468.

(11) Yu, L.; Xu, H.; Monro, T. M.; Lancaster, D. G.; Xie, Y.; Zeng, H.; Chen, G. Y.; Liu, X. Ultrafast colorimetric humidity-sensitive polyelectrolyte coating for touchless control. *Mater. Horiz.* **2017**, *4*, 72−82.

(12) Lee, J. H.; Fan, B.; Samdin, T. D.; Monteiro, D. A.; Desai, M. S.; Scheideler, O.; Jin, H.-E.; Kim, S.; Lee, S.-W. Phage-Based Structural Color Sensors and Their Pattern Recognition Sensing System. *ACS Nano* **2017**, *11*, 3632−3641.

(13) Li, Z.; Fang, M.; LaGasse, M. K.; Askim, J. R.; Suslick, K. S. Colorimetric Recognition of Aldehydes and Ketones. *Angew. Chem., Int. Ed.* **2017**, *56*, 9860−9863.

(14) Im, H.; Hong, S.; Lee, Y.; Lee, H.; Kim, S. A Colorimetric Multifunctional Sensing Method for Structural-Durability-Health Monitoring Systems. *Adv. Mater.* **2019**, *31*, 1807552.

(15) Chi, H.; Liu, Y. J.; Wang, F.; He, C. Highly Sensitive and Fast Response Colorimetric Humidity Sensors Based on Graphene Oxides Film. *ACS Appl. Mater. Interfaces* **2015**, *7*, 19882−19886.

(16) Wang, Z.; Lee, J. H.; Lu, Y. Label-Free Colorimetric Detection of Lead Ions with a Nanomolar Detection Limit and Tunable Dynamic Range by using Gold Nanoparticles and DNAzyme. *Adv. Mater.* **2008**, *20*, 3263−3267.

(17) Topcu, G.; Guner, T.; Inci, E.; Demir, M. M. Colorimetric and plasmonic pressure sensors based onpolyacrylamide/Au nanoparticles. *Sens. Actuators, A* **2019**, *295*, 503−511.

(18) Cai, Z.; Smith, N. L.; Zhang, J.-T.; Asher, S. A. Two-Dimensional Photonic Crystal Chemical and Biomolecular Sensors. *Anal. Chem.* **2015**, *87*, 5013−5025.

(19) Shang, L.; Zhang, W.; Xu, K.; Zhao, Y. Bio-inspired intelligent structural color materials. *Mater. Horiz.* **2019**, *6*, 945−958.

(20) Li, M.; Gou, H.; Al-Ogaidi, I.; Wu, N. Nanostructured Sensors for Detection of Heavy Metals: A Review. *ACS Sustainable Chem. Eng.* **2013**, *1*, 713−723.

(21) Wang, H.; Zhang, K.-Q. Photonic Crystal Structures with Tunable Structure Color as Colorimetric Sensors. *Sensors* **2013**, *13*, 4192−4213.

(22) Hao, N.; Lu, J.; Zhou, Z.; Hua, R.; Wang, K. A pH-Resolved Colorimetric Biosensor for Simultaneous Multiple Target Detection. *ACS Sens.* **2018**, *3*, 2159−2165.

(23) Hong, J. I.; Chang, B.-Y. Development of the smartphone-based colorimetry for multi-analyte sensing arrays. *Lab Chip* **2014**, *14*, 1725−1732.

(24) La, Y.-K.; Hong, J.-A.; Jeong, Y.-J.; Lee, J. A 1,8-naphthalimide-based chemosensor for dualmode sensing: colorimetric and fluorometric detection of multiple analytes. *RSC Adv.* **2016**, *6*, 84098−84105.

(25) Arora, P. Colorimetric Sensors Using Hybrid Mode Plasmon Imaging for Refractive Index and Thickness Sensing. Ph.D. Thesis, Indian Institute of Technology Madras (IIT), Chennai, India, May 2017.

(26) King, N. S.; Liu, L.; Yang, X.; Cerjan, B.; Everitt, H. O.; Nordlander, P.; Halas, N. J. Fano Resonant Aluminum Nanoclusters for Plasmonic Colorimetric Sensing. *ACS Nano* **2015**, *9*, 10628−10636.

(27) Khorasaninejad, M.; Abedzadeh, N.; Walia, J.; Patchett, S.; Saini, S. S. Color Matrix Refractive Index Sensors Using Coupled Vertical Silicon Nanowire Arrays. *Nano Lett.* **2012**, *12*, 4228−4234.

(28) Hawkeye, M. M.; Brett, M. J. Optimized Colorimetric Photonic-Crystal Humidity Sensor Fabricated Using Glancing Angle Deposition. *Adv. Funct. Mater.* **2011**, *21*, 3652−3658.

(29) Chiappelli, M. C.; Hayward, R. C. Photonic Multilayer Sensors from Photo-Crosslinkable Polymer Films. *Adv. Mater.* **2012**, *24*, 6100−6104.

(30) Kats, M. A.; Blanchard, R.; Genevet, P.; Capasso, F. Nanometre optical coatings based on strong interference effects in highly absorbing media. *Nat. Mater.* **2013**, *12*, 20−24.

(31) Yoo, Y. J.; Lim, J. H.; Lee, G. J.; Jang, K.-I.; Song, Y. M. Ultra-thin films with highly absorbent porous media fine-tunable for coloration and enhanced color purity. *Nanoscale* **2017**, *9*, 2986−2991.

(32) Ko, J. H.; Yoo, Y. J.; Kim, Y. J.; Lee, S.-S.; Song, Y. M. Flexible, Large-Area Covert Polarization Display Based on Ultrathin Lossy Nanocolumns on a Metal Film. *Adv. Funct. Mater.* **2020**, *30*, 1908592.

(33) Ohta, N.; Robertson, A., Evolution of CIE Standard Colorimetric System. *Colorimetry: Fundamentals and Applications*; John Wiley & Sons: Hoboken, NJ, USA, 2006; pp 176−228.

(34) Garahan, A.; Pilon, L.; Yin, J.; Saxena, I. Effective optical properties of absorbing nanoporous and nanocomposite thin films. *J. Appl. Phys.* **2007**, *101*, No. 014320.

(35) Kim, D. H.; Yoo, Y. J.; Ko, J. H.; Kim, Y. J.; Song, Y. M. Standard red green blue (sRGB) color representation with a tailored dual-resonance mode in metal/dielectric stacks. *Opt. Mater. Express* **2019**, *9*, 3342−3351.

(36) Kats, M. A.; Sharma, D.; Lin, J.; Genevet, P.; Blanchard, R.; Yang, Z.; Qazilbash, M. M.; Basov, D. N.; Ramanathan, S.; Capasso, F. Ultra-thin perfect absorber employing a tunable phase change material. *Appl. Phys. Lett.* **2012**, *101*, 221101.

(37) Oh, J.-W.; Chung, W.-J.; Heo, K.; Jin, H.-E.; Lee, B. Y.; Wang, E.; Zueger, C.; Wong, W.; Meyer, J.; Kim, C.; Lee, S.-Y.; Kim, W.-G.; Zemla, M.; Auer, M.; Hexemer, A.; Lee, S.-W. Biomimetic virus-based colourimetric sensors. *Nat. Commun.* **2014**, *5*, 3043.

(38) Kim, W.-G.; Song, H.; Kim, C.; Moon, J.-K.; Kim, K.; Lee, S.-W.; Oh, J.-W. Biomimetic self-templating optical structures fabricated by genetically engineered M13 bacteriophage. *Biosens. Bioelectron.* **2016**, *85*, 853−859.

(39) Moon, J.-S.; Kim, W.-G.; Shin, D.-M.; Lee, S.-Y.; Kim, C.; Lee, Y.; Han, J.; Kim, K.; Yoo, S. Y.; Oh, J.-W. Bioinspired M-13

bacteriophage-based photonic nose for differential cell recognition. *Chem. Sci.* **2017**, *8*, 921−927.

(40) Moharam, M. G.; Gaylord, T. K.; Grann, E. B.; Pommet, D. A. Formulation for stable and efficient implementation of the rigorous coupled-wave analysis of binary gratings. *J. Opt. Soc. Am. A* **1995**, *12*, 1068−1076.

(41) Schmidt, D.; Schubert, E.; Schubert, M., Generalized Ellipsometry Characterization of Sculptured Thin Films Made by Glancing Angle Deposition. In *Ellipsometry at the Nanoscale*; Springer: Berlin, 2013; pp 341−410, DOI: 10.1007/978-3-642-33956-1_10.

(42) Wakefield, N. G.; Sorge, J. B.; Taschuk, M. T.; Bezuidenhout, L. W.; Brett, M. J.; Sit, J. C. Control of the principal refractive indices in biaxial metal oxide films. *J. Opt. Soc. Am. A* **2011**, *28*, 1830−1840.

(43) Oliver, J. B.; Kessler, T. J.; Smith, C.; Taylor, B.; Gruschow, V.; Hettrick, J.; Charles, B. Electron-beam−deposited distributed polarization rotator for high-power laser applications. *Opt. Express* **2014**, *22*, 23883−23896.